ELSEVIER

Journal of Structural Geology 27 (2005) 1823–1837

JOURNAL OF STRUCTURAL GEOLOGY

www.elsevier.com/locate/jsg

Grain size distribution and thickness of breccia and gouge zones from thin (<1 m) strike-slip fault cores in limestone

Andrea Billi*

Dipartimento di Scienze Geologiche, Università 'Roma Tre', Largo S. L. Murialdo 1, 00146 Rome, Italy

Received 14 April 2004; received in revised form 9 May 2005; accepted 12 May 2005
Available online 15 July 2005

Abstract

Through field and laboratory analyses, the cross-sectional structure and the grain size distribution of 10 strike-slip fault cores less than 1 m thick were studied. The fault cores are exposed in Jurassic platform limestone within the Mattinata Fault zone located in the Adriatic–Apulian foreland of southern Italy. Each fault core consists of a breccia zone and a gouge zone, which differ in thickness and grain size distribution. Through the conventional sieving-and-weighting method, the grain size distribution of 20 samples of fault rocks was obtained. The distributions follow power-laws with fractal dimension (D) in the 2.00977–3.04008 range. Gouge D-values are proportional to the normalised thickness of the corresponding gouge zones. For a gouge D-value ≈ 2.2, the thickness of the corresponding gouge zone is only about 3% of the fault core thickness, whereas for a gouge D-value ≈ 3.0, the thickness of the corresponding gouge zone is almost 90% of the fault core thickness. Results from this study suggest that, with progressing fault displacement: (i) grain comminution in fault cores occurred mostly by early bulk fragmentation of grains and late grain abrasion; (ii) breccia zones were progressively incorporated into the adjacent gouge zones.

Keywords: Breccia; Gouge; Fault core; Fault rock; Grain size distribution; Strike-slip fault

1. Introduction

Fault zones consist of volumes of intensely fractured rocks (i.e. the damage zone) associated with numerous closely spaced fault surfaces (Ben-Zion and Sammis, 2003; Kim et al., 2004). The thickness of a fault zone may vary from sub-millimetres to a kilometre or more (Scholz, 1987; Sibson, 2003). Cataclastic fault zones usually include a fault core (Chester and Logan, 1986; Chester et al., 1993; Caine et al., 1996; Evans et al., 1997), which is where pre-existing rock fabrics (e.g. sedimentary and tectonic structures) are erased by the generation of fault rocks (Billi et al., 2003a; Graham et al., 2003). The development and physical attributes of fault cores and fault core rocks have been extensively studied in natural faults (Wibberley and Shimamoto, 2003), in laboratory experiments (Frye and Marone, 2002) and in numerical simulations (Abe and Mair, 2005). It is often documented that grain comminution and hence wear increase with increased fault displacement (Engelder, 1974; Mandl et al., 1977; Aydin, 1978; Hooke and Iverson, 1995; Amitrano and Schmittbuhl, 2002). It is also documented that the grain size distribution of fault rocks usually follows power-laws (Blenkinsop, 1991; Storti et al., 2003) and that the relative fractal dimension (D) increases with the number of fracturing events and hence with fault displacement (Blenkinsop, 1991; Monzawa and Otsuki, 2003). Specific D-values have been correlated with different micromechanical models of grain fragmentation, namely the 'pillar of strength' model of Allègre et al. (1982) for $D=1.97$, the 'constrained comminution' model of Sammis et al. (1987) for $D=2.58$ and the 'plane of fragility' model of Turcotte (1986) for $D=2.84$. Several data from laboratory simulations of faults (Beeler et al., 1996) show power-law grain size distributions of fault rocks with $D\approx 2.6$, thus supporting Sammis et al.'s model of constrained comminution. Sammis et al. (1986) inferred a steady-state self-similar process of cataclasis leading progressively to the development of fault gouge. However, data from natural fault rocks show a large variability of D-values, thus suggesting that the mechanisms of grain

* Tel.: +39 0654888016; fax: +39 0654888201.
E-mail address: billi@uniroma3.it.

0191-8141/$ - see front matter © 2005 Elsevier Ltd. All rights reserved.
doi:10.1016/j.jsg.2005.05.013

comminution in natural fault rocks may spatially and temporally vary and cannot be generally explained by a steady-state self-similar process (Blenkinsop, 1991; Storti et al., 2003).

Despite the wealth of data about fault cores and related rocks, to date, the structural and physical characterisation of cataclastic fault zones in carbonate rocks is still in an infant stage because of the paucity of published field data and laboratory experiments. It follows that the seismic and hydraulic properties of carbonate fault cores are poorly constrained. This is in striking contrast to the vast and still increasing literature on cataclastic fault zones in crystalline rocks and siliciclastic sediments (Di Toro et al., 2004; Wilson et al., 2005). Yet carbonate sedimentary rocks frequently occur in the upper crust, where they can act as petroleum or water reservoirs (Mancini et al., 2004) as well as foci for seismic faulting (Miller et al., 2004).

In this paper, structural analyses of fault cores and fault core rocks developed across carbonate beds are presented. The exposure-scale structural architecture and the grain size distribution of 10 fault cores located within the regional strike-slip Mattinata Fault zone (Salvini et al., 1999) in the Adriatic foreland of southern Italy (Fig. 1) are analysed. The analysed fault cores are less than 1 m thick and consist of adjacent, cataclastic gouge and breccia zones (Fig. 2). Empirical relationships among physical parameters of the fault core components are discussed. Insights into the micromechanical processes of comminution as well as inferences for the growth of strike-slip fault cores in carbonate rocks are discussed.

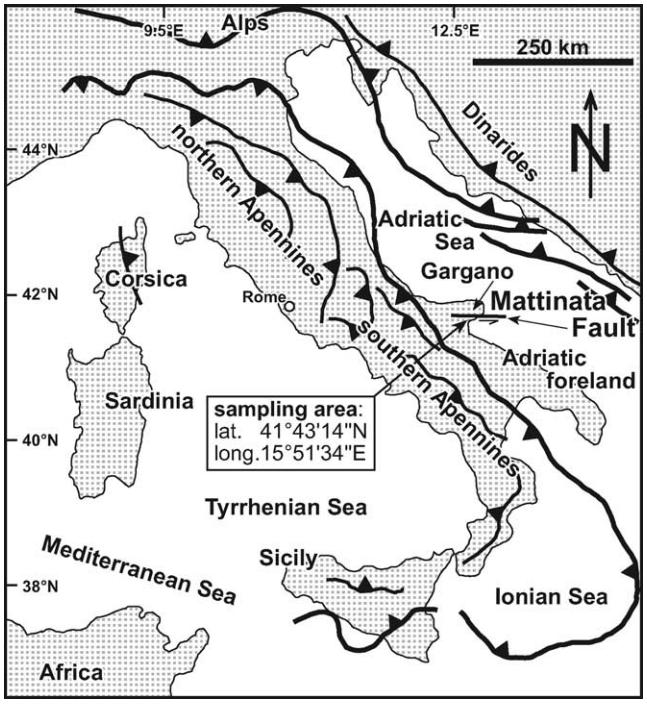

Fig. 1. Schematic tectonic setting of Italy and location for the studied fault cores within the strike-slip Mattinata Fault zone in the Adriatic–Apulian foreland.

The results presented in this paper expand from those of previous studies (Salvini et al., 1999; Billi et al., 2003a,b; Storti et al., 2003; Billi and Storti, 2004) and place further constraints on models for the growth of cataclastic fault zones thereby discussed. In particular, Salvini et al. (1999) and Billi et al. (2003a) addressed the structural (i.e. fracture) architecture of damage zones and damage zone-fault core transitional zones in carbonate beds from extensional and strike-slip fault zones, including the Mattinata Fault zone. Storti et al. (2003) addressed the non-self-similar evolution of cataclasis in both extensional and strike-slip fault cores in carbonate beds. They also drew conclusions about the micromechanical processes (i.e. bulk fragmentation versus abrasion) of grain comminution. Billi et al. (2003b) empirically correlated a set of D-values obtained from the power-law grain size distributions of carbonate fault rocks with the transpressional angles of the corresponding fault cores and, hence, indirectly with the stress perpendicular to the faults. Billi and Storti (2004) analysed the grain size distribution of fault rocks from a thick (i.e. 26 m) strike-slip fault core within the Mattinata Fault zone and concluded that the fault core rocks evolved by different fragmentation modes both in time and in space. Unlike previous papers, the correlation between the values of D as derived from the power-law distributions of fault rock grain size and the thickness of the relative breccia and gouge zones from thin (<1 m) carbonate fault cores are hereafter addressed. This correlation led to inferences about the growth of strike-slip faults and, in particular, about the relationships between the evolution of grain comminution and the evolution of the thickness of fault core components (i.e. the breccia and gouge zones).

2. Structural setting

The fault cores were analysed on exposures located within the zone of fractured and crushed rocks that surrounds the Mattinata Fault in the Adriatic–Apulian foreland (Fig. 1). This fault was chosen for its relatively simple history of left-lateral strike-slip displacement within a foreland environment (Salvini et al., 1999). The Mattinata Fault zone is exposed for more than 40 km in length and is between 200 and 300 m thick depending on the structural complexities along the fault (Brankman and Aydin, 2004). Intensity of rock damage reduces from the middle sector of the fault zone, where several fault surfaces and associated cataclastic rocks occur, toward the edges of the fault zone, where fault-related deformations gradually fade away into a poorly deformed protolith (Salvini et al., 1999). The analysed fault cores were all exposed in the same area (i.e. same structural position along the Mattinata Fault), within the mid $\sim$80 m of the Mattinata Fault damage zone. Specifically, the fault cores were exposed along the active

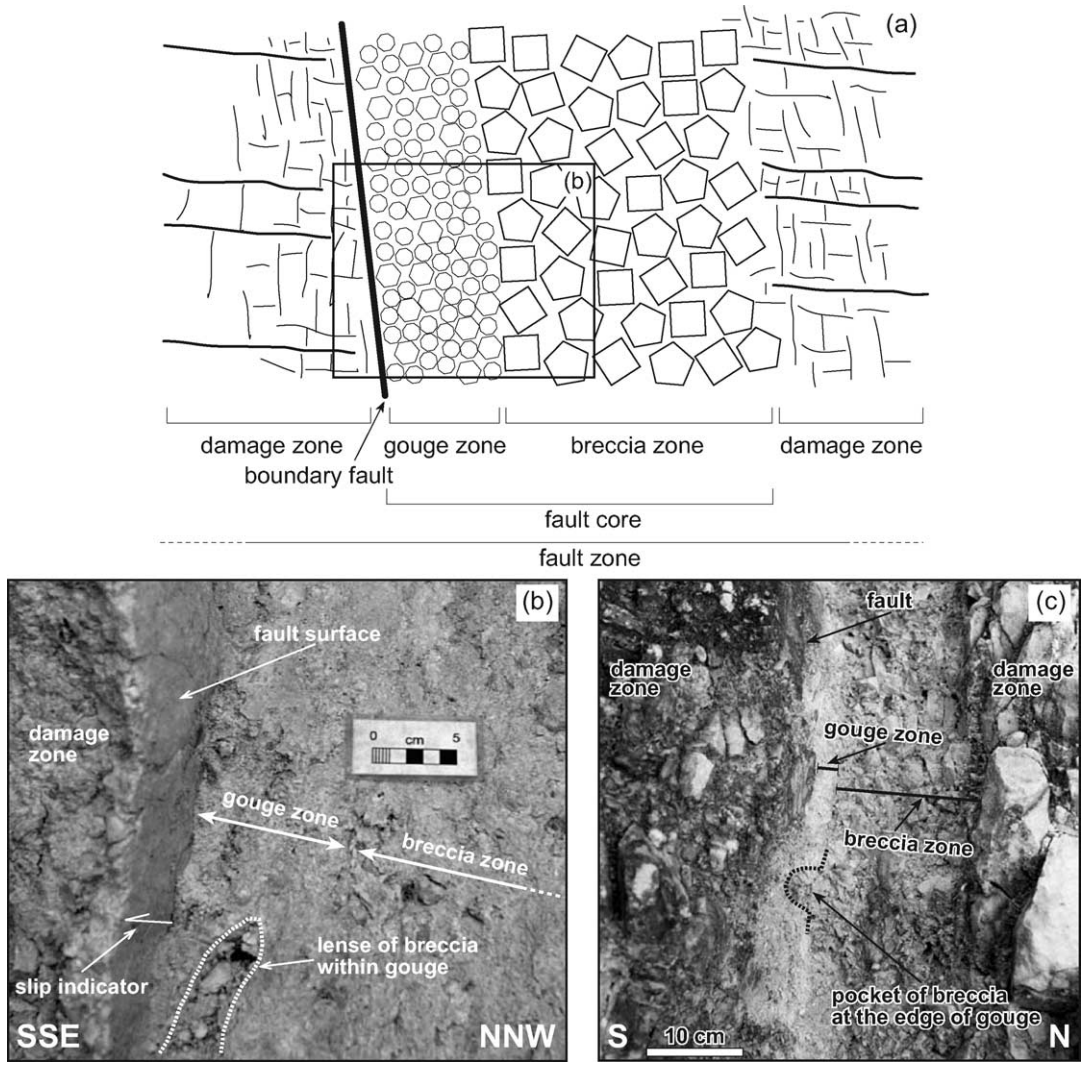

Fig. 2. (a) Conceptual cross-sectional sketch of a fault zone sectioned perpendicularly to the fault surface and to the slip direction (i.e. vertical cross-section for a strike-slip fault). The sketch shows the typical cross-sectional structure of the studied strike-slip fault cores that include a boundary fault, a gouge zone and a breccia zone. The fault core is included within a damage zone. (b) and (c) Photographs showing sections of the studied fault cores.

fronts of the S. Simeone Quarries (see area co-ordinates in Fig. 1), where Jurassic platform limestones occur. The S. Simeone Quarries are located along a slightly transcontractional segment of the Mattinata Fault where the quarries occupy an area of about 2–3 km^2. Because of the quarrying activity, some of the studied exposures were eliminated soon after the analysis hereafter reported. No structural interactions were observed among the analysed fault cores, because no intersections among them occurred on the studied exposures and because the distance among the fault cores (i.e. between a minimum of ~10 m and a maximum of several tens of metres along the fault) was much greater than their thickness.

3. Method

The fault cores were analysed on exposures perpendicular to the boundary faults and to their slip direction (Fig. 2). Before analysing the fault core exposures and collecting samples, a 20–30-cm-thick layer of surface material was removed to eliminate possibly weathered rocks. Among other parameters such as fault attitude and kinematics, the fault-perpendicular thickness of gouge and breccia zones (Fig. 2) was measured directly on the exposures (Table 1). Measured thicknesses were averaged over the fault exposure by using a thin string properly pinned along the edge of gouge and breccia zones. This method allowed measurement of the thickness of fault core components with an error usually less than 1 cm (i.e. the difference between local thickness and the average one). In the case of very narrow gouge and breccia zones (i.e. less than 5 cm in thickness, see Table 1), thickness measurements were particularly careful and errors were set at less than 0.5 cm. In each fault core, one sample was collected from the breccia zone and one sample from the gouge zone, making a total of 20 samples (Table 1).

Table 1
List of fault core data

Fault core	Fault azimuth (°)	Kinematics	Gouge sample	Breccia sample	Gouge zone thickness (m)	Breccia zone thickness (m)	Fault core thickness (m)
F01	N123	Strike-slip	SSIM01	SSIM02	0.055	0.050	0.105
F02	N094	Strike-slip	SSIM03	SSIM04	0.030	0.005	0.035
F03	N137	Strike-slip	SSIM05	SSIM06	0.045	0.095	0.140
F04	N156	Strike-slip	SSIM07	SSIM08	0.020	0.740	0.760
F05	N074	Strike-slip	SSIM09	SSIM10	0.065	0.015	0.080
F06	N152	Strike-slip	SSIM11	SSIM12	0.415	0.520	0.935
F07	N179	Strike-slip	SSIM13	SSIM14	0.040	0.070	0.110
F08	N008	Strike-slip	SSIM15	SSIM16	0.035	0.325	0.360
F09	N099	Strike-slip	SSIM17	SSIM18	0.040	0.035	0.075
F10	N154	Strike-slip	SSIM19	SSIM20	0.155	0.580	0.735

To know the general geometry and the deformational state of fault rock grains, microscopic observations were made on thin-sections obtained from fault rock samples properly embedded in epoxy resins.

The grain size distributions of fault rock samples were determined by the conventional sieving-and-weighting method (Krumbein and Pettijohn, 1938) properly adapted to the analysed material (Storti et al., 2003). In particular, (1) the samples were disaggregated in a non-destructive ultrasonic device (Vibra-Cell by Sonics & Materials Inc., Danbury CT, USA) and sieved through seven sieves with standard mesh apertures of 4.0, 2.0, 1.0, 0.5, 0.25, 0.125, and 0.063 mm; (2) the dry residue in each sieve was weighted by using a precision balance (HF-1200G by A&D Company Limited, Tokyo, Japan) with a resolution of 0.01 g; (3) by assuming a nearly spherical shape of fault rock grains (Hooke and Iverson, 1995), for each size class of each sample, the number of equivalent spherical grains (Table 2) was determined by dividing the weight of the residue in each sieve into the weight of a sphere with the density of 2670 kg m^{-3} (i.e. the limestone density) and the radius equal to half the mesh aperture of the next upper sieve. In the computation of the number of equivalent spherical grains, the use of different reference weights (i.e. such as the weight of the sphere with the same diameter as the mesh aperture of the underlying sieve, or the weight of the sphere having the average diameter between the mesh apertures of adjacent sieves) does not affect the final distribution of the resulting equivalent grain numbers. To avoid a possible bias of the distribution toward coarse grains, the residue in the sieve with the largest mesh aperture (4.0 mm) was not considered; (4) the numbers of equivalent spherical grains were plotted versus the corresponding size classes on log–log graphs; and (5) best-fits to these data were found using the following power-law relationship:

$$\log(y) = -D\log(x) + A \quad (1)$$

Table 2
List of numbers of equivalent spherical grains sorted by grain size (i.e. 4.0, 2.0, 1.0, 0.5, 0.25 and 0.125 mm)

Fault core	Sample	Grain no. (4.0 mm)	Grain no. (2.0 mm)	Grain no. (1.0 mm)	Grain no. (0.5 mm)	Grain no. (0.25 mm)	Grain no. (0.125 mm)
F01	SSIM01 (gouge)	50	317	2051	13,755	98,597	482,057
F01	SSIM02 (breccia)	218	936	3972	19,564	111,816	986,546
F02	SSIM03 (gouge)	69	732	6474	55,372	392,215	2,638,267
F02	SSIM04 (breccia)	216	1881	13,491	93,719	608,523	3,481,066
F03	SSIM05 (gouge)	187	1118	6024	34,464	183,862	961,368
F03	SSIM06 (breccia)	304	1592	6160	21,775	87,197	367,611
F04	SSIM07 (gouge)	358	2129	10,424	48,262	206,694	861,568
F04	SSIM08 (breccia)	586	4339	20,790	67,649	209,416	776,723
F05	SSIM09 (gouge)	47	496	4606	37,911	250,642	1,718,101
F05	SSIM10 (breccia)	126	821	5236	33,154	204,519	1,274,499
F06	SSIM11 (gouge)	261	1695	11,112	70,565	399,940	2,336,123
F06	SSIM12 (breccia)	126	918	6085	37,096	203,890	1,020,423
F07	SSIM13 (gouge)	112	985	6533	37,589	184,377	837,305
F07	SSIM14 (breccia)	245	1359	6751	32,596	146,952	613,902
F08	SSIM15 (gouge)	341	1840	9057	42,496	204,291	934,358
F08	SSIM16 (breccia)	408	2029	8448	36,659	159,312	722,857
F09	SSIM17 (gouge)	55	432	3213	19,848	122,149	736,857
F09	SSIM18 (breccia)	284	1387	6265	28,357	157,265	882,922
F10	SSIM19 (gouge)	432	2916	16,432	83,533	399,368	1,713,523
F10	SSIM20 (breccia)	685	3573	15,995	66,259	276,965	1,155,472

where x is the grain size class (i.e. the grain diameter in this paper) and y is the number of equivalent spherical grains in that grain size class. Eq. (1) is linear in log–log space and D is the fractal dimension, i.e. the slope of the best-fit line. In this type of analysis, D can be considered as a measure of the relative abundance of small and coarse grains in each sample, with D-values increasing with increases in the relative abundance of small grains (e.g. Blenkinsop, 1991).

Reproducibility of results through the sieving-and-weighting method described above is documented in a previous paper (Storti et al., 2003).

4. Results

4.1. Structure and thickness of fault core components

All analysed fault cores have the same asymmetrical cross-sectional structure, which includes, from one side to the other: a boundary polished fault surface, a gouge zone along the boundary fault, and a breccia zone near the gouge zone (Figs. 2 and 3). This asymmetrical structure is common to most fault cores in carbonate rocks, regardless of fault kinematics (Billi et al., 2003a; Storti et al., 2003). The fault-perpendicular thickness of the analysed fault cores (i.e. gouge zone thickness plus breccia zone thickness) varies between a minimum of 0.070 m and a maximum of 0.935 m (Table 1). The thickness of gouge zones varies between a minimum of ~3% and a maximum of ~86% of the fault core thickness (Table 1). Gouge and breccia zones are sub-vertical bands of incoherent to poorly coherent fault rocks. They show striking contrast in grain size distributions (Fig. 3a–d). Grains of gouge zones are generally less than 1 mm in size, whereas breccia zones contain several grains even coarser than 1 cm. Coarse survivor grains occur both in the gouge zones and in the breccia zones. These grains are typically rounded or sub-rounded (Fig. 3e). Lenses and pockets of coarse material within both the gouge zones and the breccia zones are common features in all the fault cores (Figs. 2b and c and 3f). The transition from the gouge zone to the breccia zone and from the breccia zone to the damage zone is usually sharp (Fig. 3b and d), although in some cases transitional material occurs along these boundaries (Fig. 3a, c and d).

Fault cores are embedded in the damage zone that consists of intensely fractured limestone beds ranging in

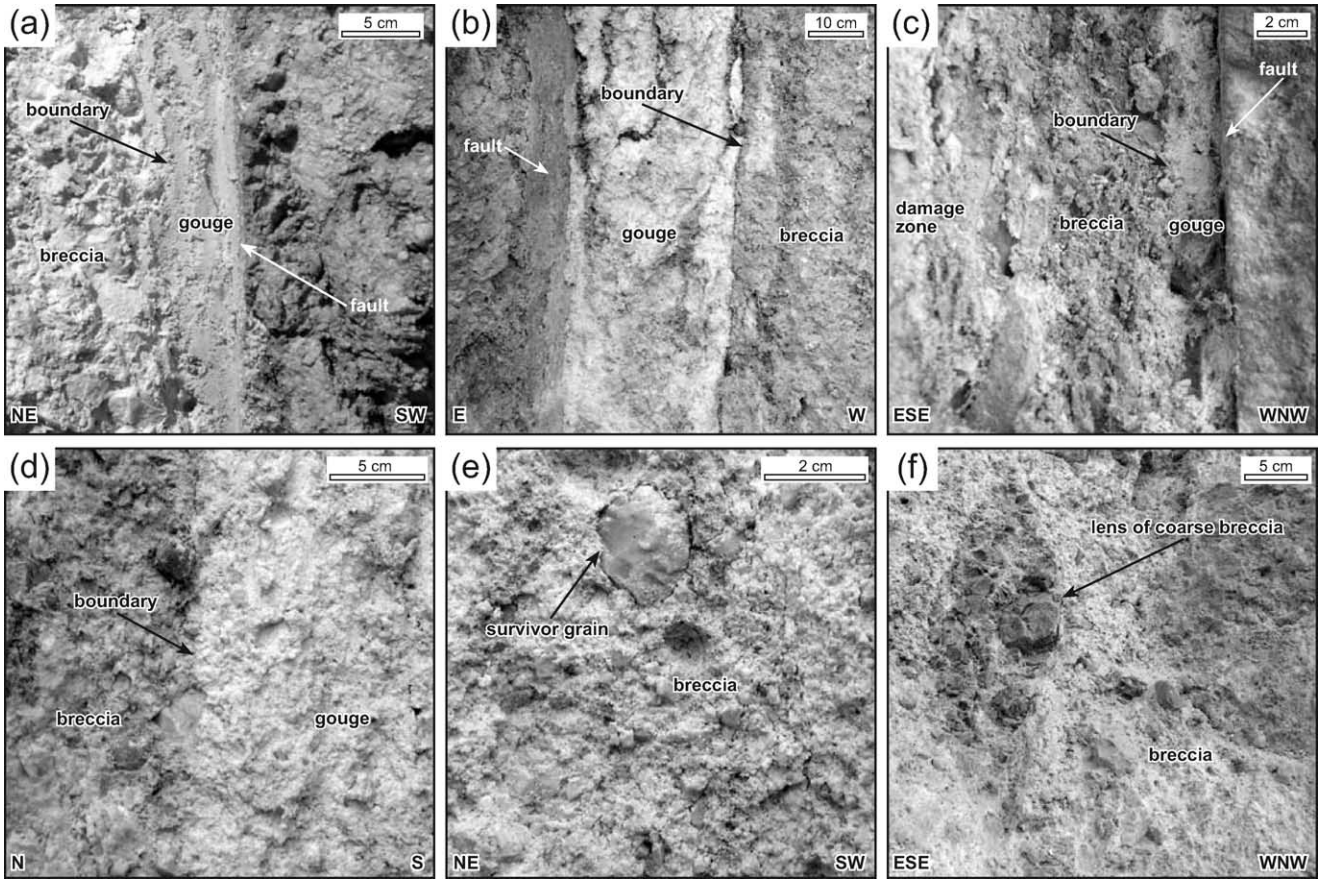

Fig. 3. Photographs of fault cores from the study site within the Mattinata Fault zone. (a) Note the different textures of breccia and gouge. (b) Note the sharp boundary between breccia and gouge zones. (c) Note the different textures of breccia, gouge and damage zones. (d) Note the sharp boundary between breccia and gouge zones and some survivor grains at the breccia–gouge boundary. (e) Note the sub-rounded survivor grain embedded in a fine matrix. (f) Note the lens of coarse breccia within smaller breccia material.

thickness between 0.3 and 2 m. In the damage zone, pre-existing sedimentary and tectonic fabrics (e.g. bedding, compaction stylolites, tectonic cleavage) are mostly preserved. Chemical analyses performed on the limestone forming the damage zone near the analysed fault cores show that this rock is composed of 95.6% $CaCO_3$, 2.7% $MgCO_3$ and 1.7% insoluble residue (i.e. sample GA in fig. 1 of Storti et al., 2003).

4.2. Microscopic observations

Six samples of fault rocks were collected in the following fault core components for thin-sectioning (Fig. 4): the breccia zones of the F04, F08 and F10 fault cores, and the gouge zones of the F01, F03 and F06 fault cores (Table 1). Three differently oriented thin-sections were made from each sample, for a total of 18 analysed thin-sections. Because of the incoherent state of fault rocks forming the studied fault cores, thin-sectioning was possible only on samples collected in rare, fairly cemented portions of the fault cores where grains were in general coarser than those occurring in the rest of the fault core. For this reason, these samples may be poorly representative of the size distribution and deformational state of the fault core in which they were collected. These samples are probably representative of a deformational state earlier than the one characteristic of the surrounding fault core.

Fig. 4 shows a selection of microphotographs from fault rock thin-sections. Fig. 4a shows a fault rock (i.e. from the F08 fault core) consisting of angular coarse grains. A fine matrix is almost absent and the grain size is well sorted. Grains have a near-rectangular, elongate shape with the long axis at least 1.5 times greater than the short axis. Fractures are frequent and break apart the bulk of the elongate grains.

Fig. 4b and c shows a fault rock (i.e. from the F03 fault core) consisting of coarse grains, which are partly embedded in a fine matrix and partly in contact with one another. The grain size is fairly (Fig. 4b) to poorly (Fig. 4c) sorted. Coarse grains are more rounded than those occurring in Fig. 4a. Fractures are frequent and cut across the bulk of coarse grains.

Fig. 4d and e (Fig. 4e is a magnification of the portion of Fig. 4d within the inset) shows a fault rock (i.e. from the F03 fault core) consisting of coarse grains embedded in a fine matrix and occasionally in contact with one another. The grain size distribution is poorly sorted. Most coarse grains are sub-rounded. Fractures break off asperities occurring along the edges of sub-rounded grains or cut across the bulk of grains when these are elongate and not rounded.

Fig. 4f shows a near-pentagonal grain (i.e. from the F06

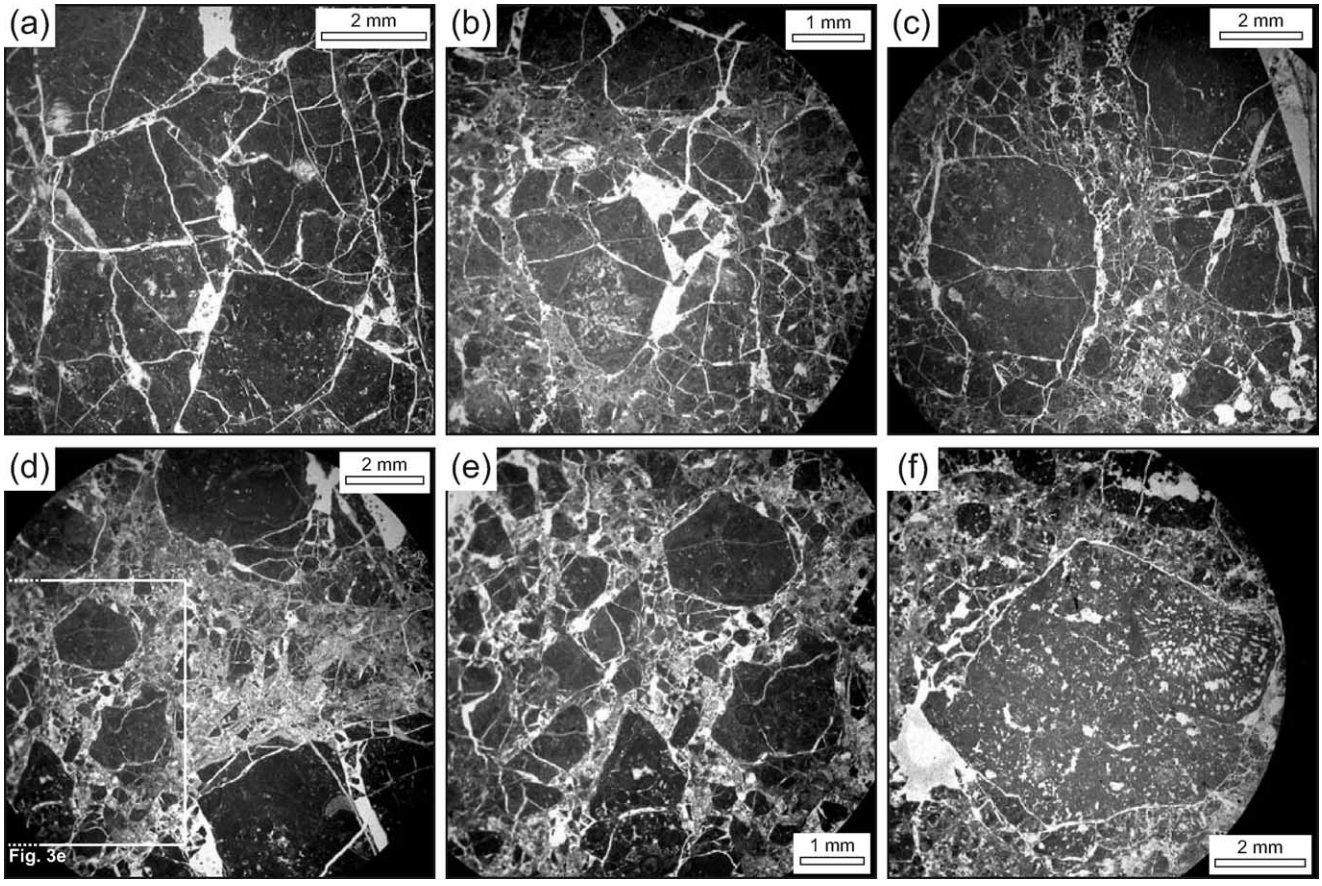

Fig. 4. Photographs of thin-sections from fault rock samples collected in the studied fault cores (see the text for explanations).

fault core) embedded in a fine matrix. Fractures occur along the edges of the grain and break off chips and slabs (i.e. asperities). No fractures cut across the bulk of the grain. Note the fossil of a Jurassic alga (i.e. *Cayeuxia*) included in the grain.

In the analysed thin-sections, no stylolites or other evidence of dissolution processes were observed.

4.3. Grain size distribution of fault rocks

The numbers of equivalent spherical grains (Table 2) plotted against the corresponding grain diameters on log–log graphs follow linear trends (Fig. 5) and are well-fitted by Eq. (1) in the 4.000–0.125 mm size range (Table 3). The relative fractal dimension D varies between $\sim$2.009 and $\sim$2.791 for the breccia samples, and between $\sim$2.233 and $\sim$3.040 for the gouge samples. In each fault core, the ratio between gouge and breccia D-values is $\sim$1.1. Gouge and breccia D-values correlate with the corresponding weight of grains smaller than 0.063 mm as divided by the total weight of the sample (i.e. $W_{<63}/W_{tot}$ in Fig. 6). Specifically, for $D \approx 2$, the weight of the material with grain size smaller than 0.063 mm corresponds to less than 1% of the sample total weight, whereas for $D \approx 3$, the weight of the material with grain size smaller than 0.063 mm increases to more than 30% of the sample total weight (Fig. 6). Grains less than 0.063 mm in size are out of the size range considered for the computation of D-values (Fig. 5).

To study possible evolutionary relationships between breccia and gouge zones, the weight-normalised numbers were compared for grains of the same size from adjacent gouge and breccia samples (i.e. same fault core) (Fig. 7). Specifically, for each size class of each sample, the number of equivalent grains appropriate for 1000 g of standard sampled material was computed. Results from each size class of the gouge samples were then divided by the results from the corresponding size class of the adjacent breccia samples. These ratios were plotted against the corresponding grain size classes (Fig. 7). Fig. 7 shows that the number of grains in the 4 mm size class is approximately the same in all the sample pairs, i.e. the grain ratios are approximately 1. In particular, in eight out of ten fault cores, the grain ratio for the 4 mm size class is slightly less than 1, that is the number of coarse grains is slightly greater in the breccia zones than in the adjacent gouge zones. In the remaining two cases, this ratio is slightly greater than 1. For small grain size classes, the ratio between grains of the same size increases over 1, indicating that the small grains are more abundant in the gouge samples than in the adjacent breccia samples. In two cases, the number of grains in the 0.125 mm size class is between four and five times greater in the gouge sample than in the adjacent breccia sample (Fig. 7).

4.4. Thickness versus grain size distribution

Simple proportionality occurs between gouge D-values and the ratio between the thickness of gouge zones and the thickness of the relative fault cores (Fig. 8a). For $D \approx 2.2$, the gouge zone thickness is only $\sim$3% of the fault core thickness, whereas for $D \approx 3$, the gouge zone thickness increases to almost 90% of the fault core thickness. Poor inverse correlation occurs between breccia D-values and the ratio between the thickness of breccia zones and the thickness of the relative fault cores (Fig. 8b). For $D \approx 2.0$,

Table 3
List of best-fit equations (Eq. (1)) plotted in Fig. 5 and associated statistical parameters

Fault core	Sample	Power-law best-fit equation (Eq. (1))		D	R^2	Residual sum of squares	Residual mean square
F01	SSIM01 (gouge)	$\log(y) = -2.67821$	$\log(x) + 7.64097$	2.67821	0.999362	0.0384996	0.0096249
F01	SSIM02 (breccia)	$\log(y) = -2.39229$	$\log(x) + 8.47417$	2.39229	0.993766	0.3018660	0.0754664
F02	SSIM03 (gouge)	$\log(y) = -3.04008$	$\log(x) + 8.64523$	3.04008	0.998448	0.1208000	0.0302001
F02	SSIM04 (breccia)	$\log(y) = -2.79141$	$\log(x) + 9.40809$	2.79141	0.998826	0.0769736	0.0192434
F03	SSIM05 (gouge)	$\log(y) = -2.46359$	$\log(x) + 8.69642$	2.46359	0.999861	0.0071149	0.0017787
F03	SSIM06 (breccia)	$\log(y) = -2.11909$	$\log(x) + 8.84752$	2.11909	0.999887	0.0042704	0.0010676
F04	SSIM07 (gouge)	$\log(y) = -2.23357$	$\log(x) + 9.14028$	2.23357	0.998397	0.0673283	0.0168321
F04	SSIM08 (breccia)	$\log(y) = -2.00977$	$\log(x) + 9.57478$	2.00977	0.987865	0.4171990	0.1043000
F05	SSIM09 (gouge)	$\log(y) = -3.02373$	$\log(x) + 8.25460$	3.02373	0.997986	0.1551420	0.0387854
F05	SSIM10 (breccia)	$\log(y) = -2.65946$	$\log(x) + 8.54552$	2.65946	0.999971	0.0017069	0.0004267
F06	SSIM11 (gouge)	$\log(y) = -2.62713$	$\log(x) + 9.26345$	2.62713	0.999719	0.0163044	0.0040761
F06	SSIM12 (breccia)	$\log(y) = -2.59650$	$\log(x) + 8.59332$	2.59650	0.998574	0.0809246	0.0202312
F07	SSIM13 (gouge)	$\log(y) = -2.55742$	$\log(x) + 8.56249$	2.55742	0.995508	0.2481170	0.0620292
F07	SSIM14 (breccia)	$\log(y) = -2.25731$	$\log(x) + 8.74257$	2.25731	0.999079	0.0395005	0.0098751
F08	SSIM15 (gouge)	$\log(y) = -2.27763$	$\log(x) + 9.05938$	2.27763	0.999729	0.0118158	0.0029539
F08	SSIM16 (breccia)	$\log(y) = -2.14164$	$\log(x) + 9.03231$	2.14164	0.999793	0.0079825	0.0019956
F09	SSIM17 (gouge)	$\log(y) = -2.73158$	$\log(x) + 7.93159$	2.73158	0.999112	0.0557459	0.0139365
F09	SSIM18 (breccia)	$\log(y) = -2.30469$	$\log(x) + 8.79057$	2.30469	0.999166	0.0372766	0.0093191
F10	SSIM19 (gouge)	$\log(y) = -2.38318$	$\log(x) + 9.56364$	2.38318	0.997829	0.1038930	0.0259732
F10	SSIM20 (breccia)	$\log(y) = -2.12803$	$\log(x) + 9.59307$	2.12803	0.999236	0.0291127	0.0072781

D is the fractal dimension and R^2 is the coefficient of determination. (x) = size (diameter) of grains. (y) = number of equivalent spherical grains.

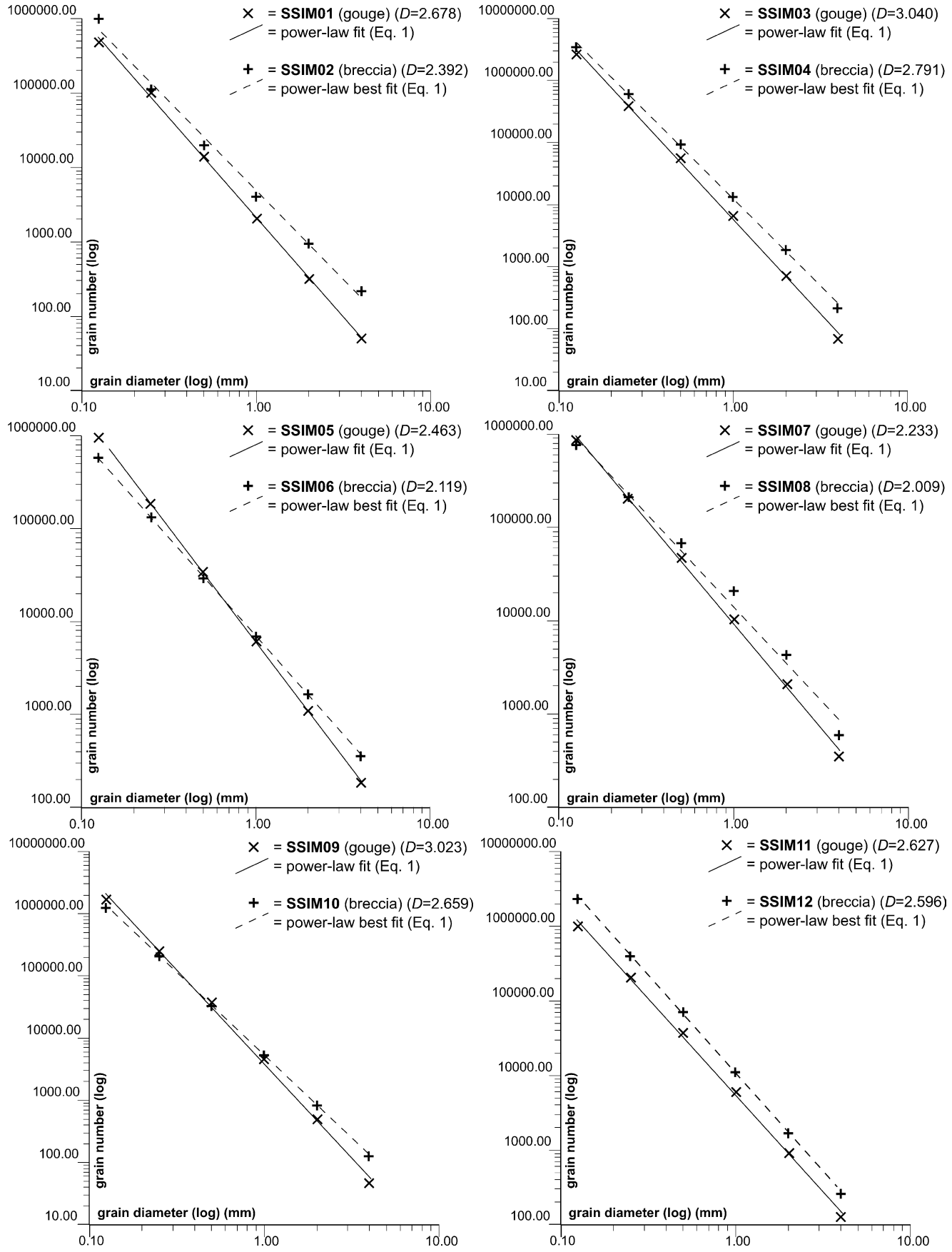

Fig. 5. Log–log graphs showing the relationship between grain size (i.e. diameter) and grain number of cataclastic rock samples collected from the analysed fault cores. Crosses are plotted data. Solid and dashed lines are the relative power-law best-fit (Eq. (1)).

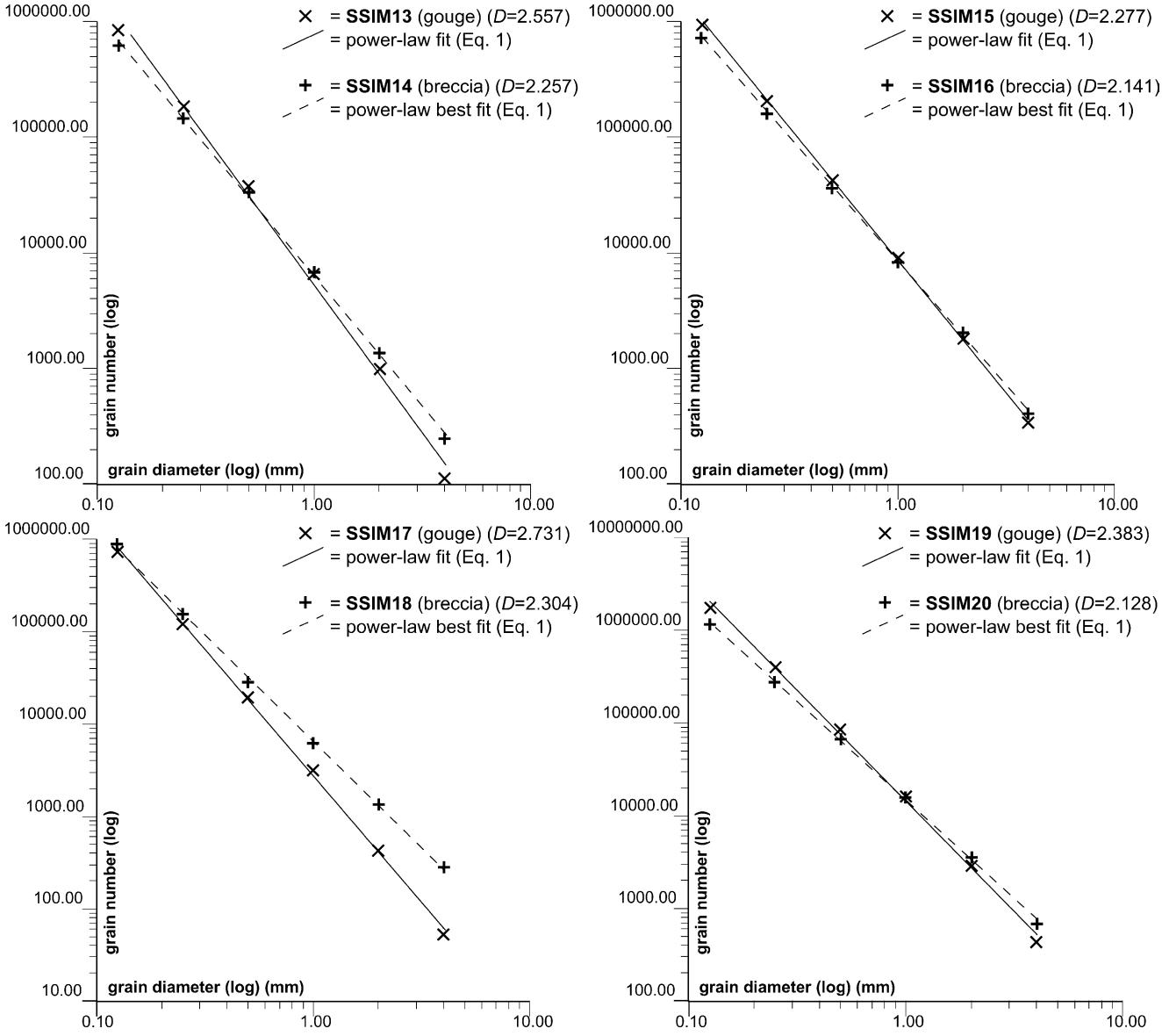

Fig. 5 (*continued*)

the breccia zone thickness is ~90% of the fault core thickness, whereas for $D \approx 2.8$, the breccia zone thickness reduces to ~15% of the fault core thickness.

5. Discussion

5.1. Insights into the micromechanical processes of comminution

The occurrence of coarse survivor grains in the breccia and gouge zones as well as the presence of pockets and lenses of breccia material within the gouge zones (Figs. 2–4) suggests that gouge rocks developed by comminution from early breccia material. The development of highly sheared gouge bands from early breccia material is a common process in brittle shear zones (Ramsay, 1980) and is documented in several natural and laboratory examples (Sammis et al., 1987; Marone and Scholz, 1989; Hattori and Yamamoto, 1999). In this work, the ratio between the weight-normalised numbers of grains from gouge and breccia sample pairs (Fig. 7) provided insights into the micromechanical processes of comminution that promoted the breccia-to-gouge evolution. Fig. 7 showed that, for the same weight of breccia and gouge materials, the number of coarse grains (i.e. >2.0 mm) is approximately the same in the breccia and gouge zones, or slightly greater in the breccia zones (Fig. 7 considers only grains ≤4 mm, although larger grains occur, in particular, in the breccia zones). On the contrary, the number of small grains (i.e. <0.25 mm) in the gouge zones can even be 400–500% that of the adjacent breccia zones. During the breccia-to-gouge

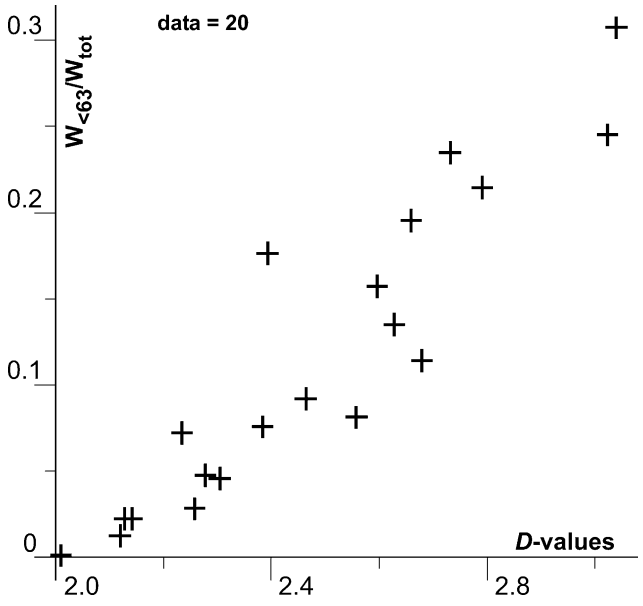

Fig. 6. Graph showing the relationship between *D*-values from the grain size distributions of fault rock samples and the relative abundance of small grains (i.e. size <0.063 mm). On the *x*-axis are *D*-values. On the *y*-axis are weights of sample grains smaller than 0.063 mm in diameter divided by the relative sample total weights ($W_{<63}/W_{tot}$).

evolution, the relative enrichment of small grains can occur substantially by two different comminution processes (Sibson, 1986; Blenkinsop, 1991; Hooke and Iverson, 1995; Morgan et al., 1996; Cladouhos, 1999; Storti et al., 2003): (1) the preferential bulk fragmentation of coarse grains (Fig. 9a) and (2) the grain abrasion (Fig. 9b). A mixed-mode process is also possible. The preferential occurrence of one of these processes depends, among other factors, on the size distribution and spatial arrangement of grains, because bulk fragmentation of grains occurs more easily when same-sized coarse grains are in contact with one another (Turcotte, 1986; Sammis et al., 1987) and form, for example, bridges (Fig. 9a) (Hooke and Iverson, 1995). The bulk fragmentation of grains implies a significant reduction in the number of coarse grains (Fig. 4a–c). On the contrary, grain abrasion becomes predominant when same-sized grains tend not to be in contact with one another (Fig. 4d–f) and hence their interactions are minimised (Hooke and Iverson, 1995). Unlike bulk fragmentation of grains, the process of grain abrasion implies the development of a wide grain size distribution (i.e. poor sorting) toward small size classes. This occurs by significantly increasing the number of small grains with respect to a smaller reduction in the number of coarse grains (Fig. 4f). Mesoscopic observations on the fault cores analysed in this paper showed that the breccia zones are rich in grains even coarser than 1 cm, whereas these grains are very rare in the gouge zones (Fig. 3). This evidence together with the gouge-to-breccia grain ratio data of Fig. 7 suggests that both bulk fragmentation and abrasion of grains contributed to the development of the fault cores and, specifically, of the gouge zones. This is also supported by microscopic analyses on thin-sections (Fig. 4). Bulk fragmentation was probably active in the breccia zones and, therefore, predominantly in the early stages of cataclasis (e.g. Fig. 4a and b), when the grain size distribution was characterised by abundant grains coarser than 1 cm and by low *D*-values (i.e. $D\approx$ or <2). In such a distribution, the

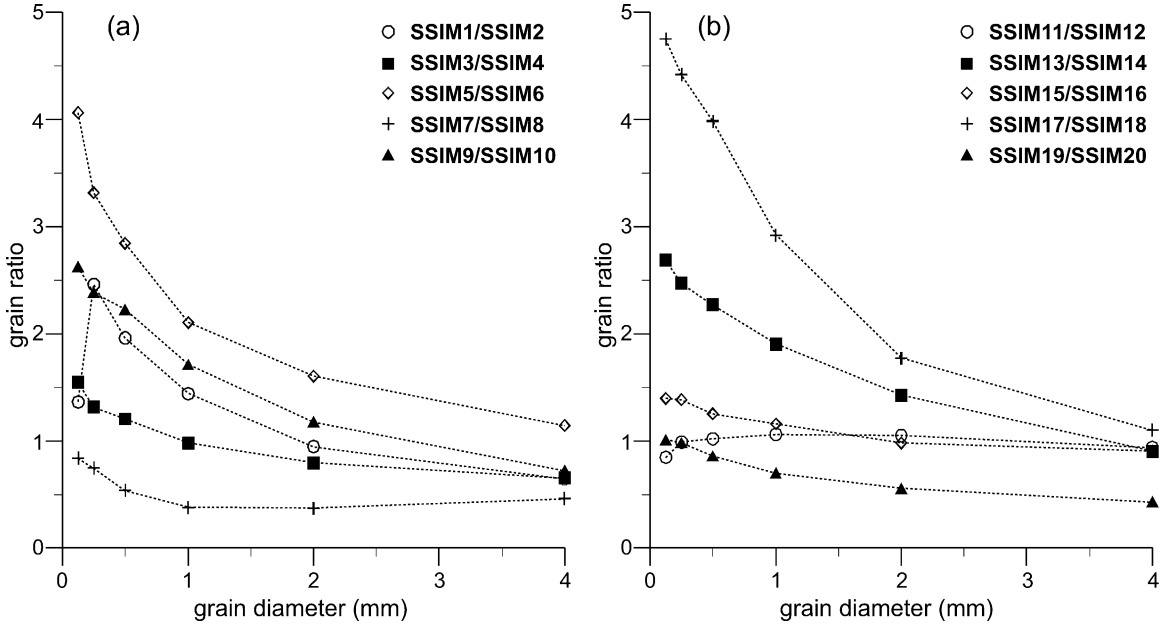

Fig. 7. Ratios between the equivalent grain numbers (weight-normalised) in the same size classes of gouge and breccia sample pairs collected in the same fault cores, plotted versus the corresponding size classes. These graphs show the relative increase/decrease of grains in each size class between adjacent gouge and breccia zones. (a) Ratios between samples SSIM01 and SSIM02, SSIM03 and SSIM04, SSIM05 and SSIM06, SSIM07 and SSIM08, and SSIM09 and SSIM10. (b) Ratios between samples SSIM11 and SSIM12, SSIM13 and SSIM14, SSIM15 and SSIM16, SSIM17 and SSIM18, and SSIM19 and SSIM20.

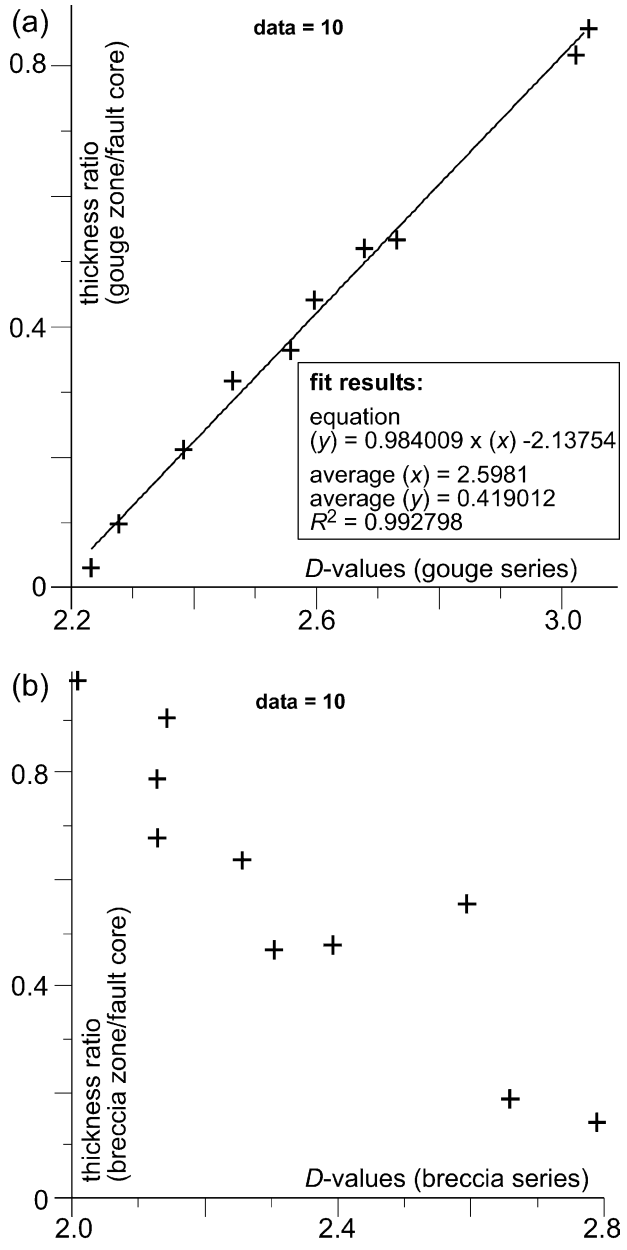

Fig. 8. (a) *D*-values from gouge samples (*x*-axis) plotted against the ratios between the thickness of the gouge zones and the thickness of the corresponding fault cores (*y*-axis). Solid line is the linear best-fit of data. (b) *D*-values from breccia samples (*x*-axis) plotted against the ratios between the thickness of the breccia zones and the thickness of the corresponding fault cores (*y*-axis).

probability of contact among coarse grains is increased and their bulk fragmentation is enhanced (Allègre et al., 1982). Most grains coarser than 1 cm were hence crushed by bulk fragmentation during the early phases of cataclasis such that these grains became very rare in the gouge zones. By progressing the grain comminution (i.e. increasing *D*-values), a fine matrix developed and gradually surrounded the survivor coarse grains such that their bulk fragmentation was progressively hindered (i.e. gouge development). At this stage, further enrichment of small grains occurred mainly by grain abrasion (Fig. 4f). Sammis et al. (1987) found that, during cataclasis, the systematic elimination of same-sized nearest neighbours leads to a theoretical grain size distribution with $D = 2.58$, in which, at all scales, grains are surrounded by no same-sized grains. This suggests that, in the analysed fault cores, while bulk fragmentation may have prevailed for fault rock grain populations with low *D*-values (i.e. breccia), grain abrasion should have progressively prevailed as *D* approached or exceeded 2.58 (i.e. gouge). Images from thin-sections of Fig. 4 suggest that, although bulk fragmentation was predominant during early cataclasis, also the grain abrasion occurred during this phase (Fig. 4d).

5.2. Inferences for the growth of fault cores

Upon the reasonable assumption of a direct relationship between comminution of fault rocks (i.e. increasing *D*-values; e.g. Marone and Scholz, 1989; Blenkinsop, 1991) and fault displacement (House and Gray, 1982a,b; Amitrano and Schmittbuhl, 2002), speculative models of fault core growth are hereafter proposed.

The proportionality between gouge *D*-values and the corresponding gouge zone to fault core thickness ratio (Fig. 8a) suggests that, with increasing fault displacement, the gouge zones grew in thickness by progressively incorporating the adjacent breccia zones (Fig. 9c and d), i.e. part of the breccia material forming the breccia zones gradually comminuted into gouge material (Wibberley et al., 2000). The data analysed in this work do not allow a distinction between whether the progressive thickening of the gouge zones occurred within fault cores whose thickness remained nearly constant (Fig. 9c) or, alternatively, within fault cores whose thickness progressively grew with fault displacement (Fig. 9d) (Scholz, 1987; Hull, 1988). In the second case (Fig. 9d), in order to comply with the observed proportionality between gouge *D*-values and the corresponding gouge zone to fault core thickness ratio (Fig. 8a), the breccia zone should have thickened, i.e. by incorporating the adjacent damage zone, at a rate lower than the rate at which the gouge zone thickened by incorporating the breccia zone itself. In any case, the approximately constant ratio (≈ 1.1, see Table 3) between *D*-values from grain size distributions of gouge and breccia sample pairs showed that grain comminution in the gouge and breccia zones progressed simultaneously.

The linear relationship between gouge *D*-values and the gouge zone to fault core thickness ratio (Fig. 8a) has an extrapolated upper bound for $D \approx 3.2$, for which the gouge zone to fault core thickness ratio is about 1, i.e. the breccia material has entirely comminuted into gouge material. With increasing fault displacement over this stage, at least two possible scenarios of fault core growth can be drawn (Fig. 10). (1) The first hypothesis involves thinning of the gouge zone by, for example, smearing over the fault surface (Fig. 10a) (Scott et al., 1994). With progressing fault

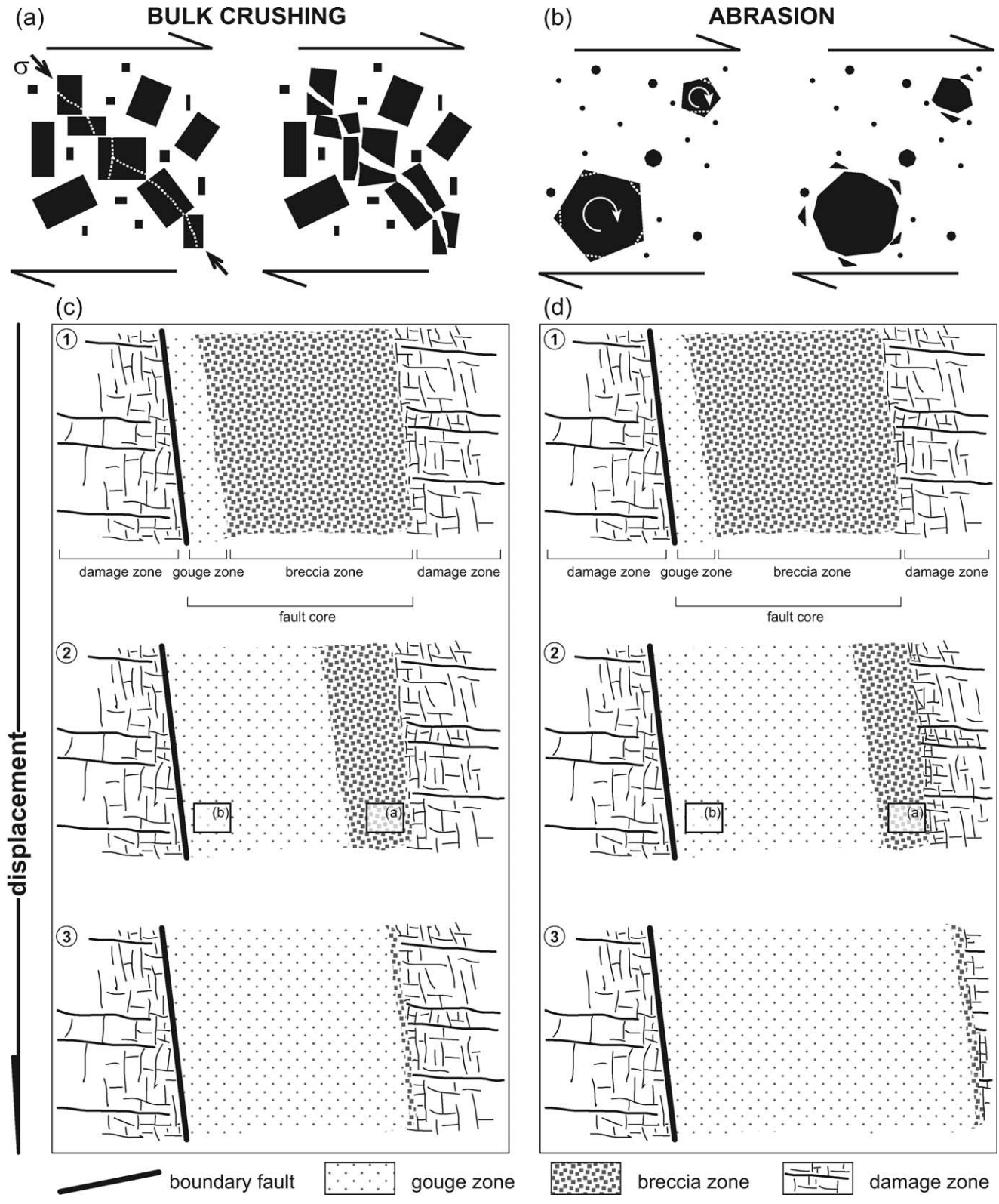

Fig. 9. (a) Conceptual sketch for the cataclastic comminution of fault rock grains by their bulk crushing. Note the formations of bridges (to the left) of coarse grains along which the stress concentrates, thus leading (to the right) to the bulk crushing of grains (Hooke and Iverson, 1995). (b) Conceptual sketch for the cataclastic comminution of fault rock grains by their surface abrasion. Angular grains (to the left) tend to rotate within a fine matrix and are accordingly abraded (to the right). (c) and (d) Conceptual sketches of a growing fault core sectioned perpendicularly to the boundary fault surface and to the shear direction (i.e. vertical cross-section for a strike-slip fault). The sequence of sketches shows the proposed evolution of the thickness of gouge and breccia zones (see the text) with increasing displacement (from top to bottom; 1, 2, 3 numbers indicate temporal succession). In (c), the fault core thickness is constant and the gouge zone thickens by gradually incorporating the near breccia zone. In (d), both the gouge zone and the breccia zone thicken, but the growth rate is greater for the gouge zone than for the breccia zone. Note insets showing locations for the comminution mechanisms sketched in (a) and (b).

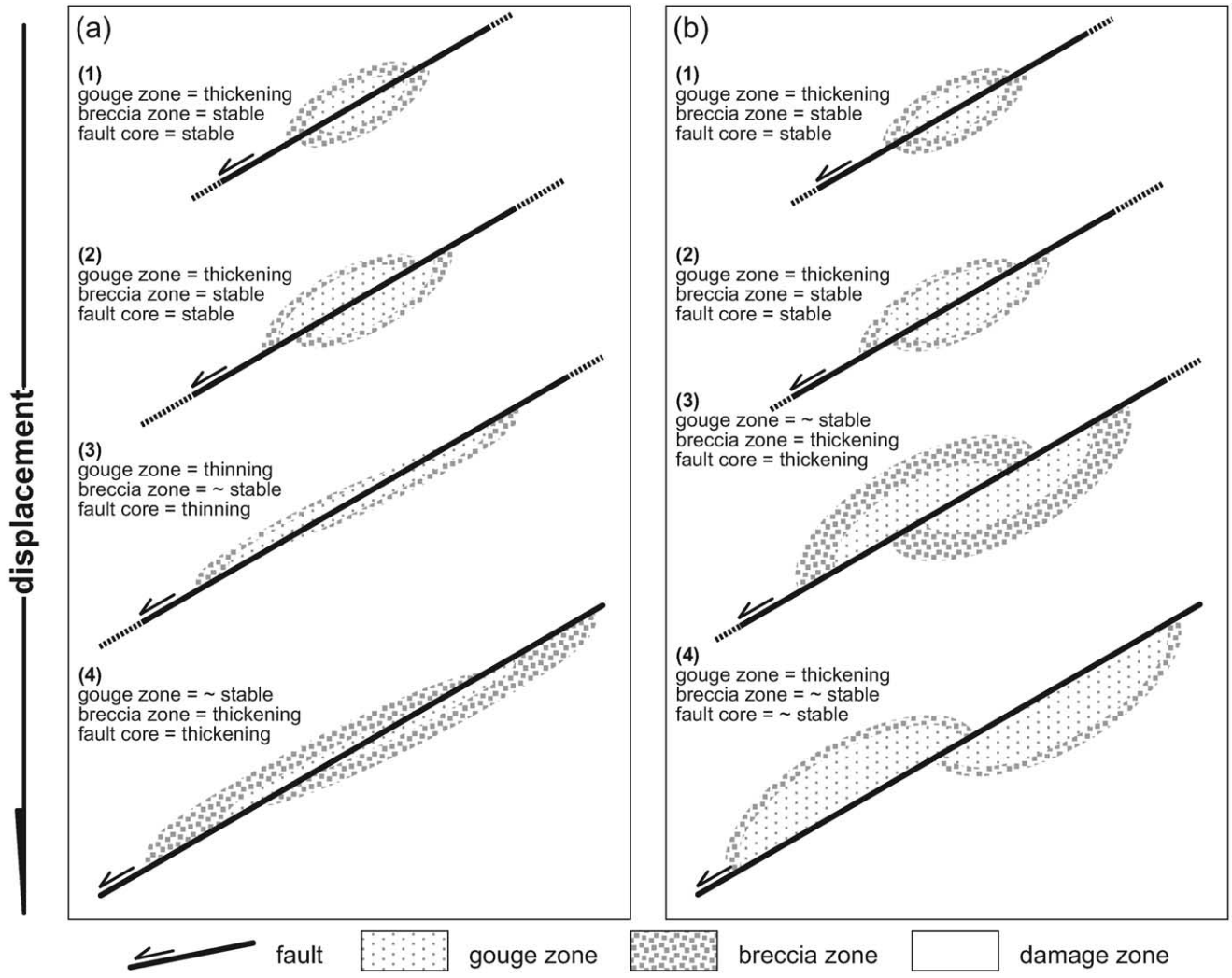

Fig. 10. Conceptual sketches of a growing fault core sectioned perpendicularly to the fault surface and parallel to the shear direction (i.e. horizontal cross-section or map view for a strike-slip fault). The succession of sketches shows two possible evolutions for the gouge and breccia zones (see text) with, from top to bottom (1, 2, 3, 4 numbers indicate temporal succession), increasing displacement. (a) In the first two stages, the fault core thickness is constant and the gouge zone thickens by gradually incorporating the near breccia zone. As displacement increases, the gouge zone thins by smearing along the fault surface (third stage). When the gouge zone is too thin for stable sliding, the fault friction renewed by the gouge thinning promotes again a thickening of the fault core (fourth stage). (b) In the first two stages, the fault core thickness is constant and the gouge zone thickens by gradually incorporating the near breccia zone. As displacement increases, the fault core keeps thickening by growing firstly the breccia zone (third stage) and, subsequently the gouge zone (fourth stage).

displacement and gouge smearing, the gouge zone may eventually thin to a lower threshold thickness, below which the stabilising effect of fault gouge on the fault slip reduces and friction significantly increases (Byerlee and Summers, 1976). Consequently, the increased fault friction may promote a new stage of fault core thickening toward the damage zone. (2) The second hypothesis involves thickening of the fault core by alternating an early thickening of the breccia zone (i.e. by incorporating the adjacent damage zone), with a subsequent thickening of the gouge zone (i.e. by incorporating the adjacent breccia zone) (Fig. 10b). However, this model fails to explain why the occurrence of a progressively thicker gouge zone, i.e. commonly characterised by lower friction properties than surrounding rocks (Beeler et al., 1996), would not prevent further fault core thickening by slip localisation mechanisms, unless the fault core strain hardens for some reason such as the progressive cementation and/or increase of rock density with grain size reduction as documented, for example, in deformation bands developed in sandstone (Aydin, 1978).

5.3. Limits and uncertainties

Results and models discussed above have limits and uncertainties that are worth discussing. The most important limit is connected with the two-dimensional characterisation of fault cores. Thickness and grain size distribution of fault cores may change along the fault strike in relation, for example, with local heterogeneities of fault strain, such as in the case of fault stepovers or jogs (Tarasewicz et al., 2005).

In this work, the along-strike structure of fault cores could not be analysed because of the lack of proper exposures. However, since the analysed fault cores were all located in the same site along the Mattinata Fault, it is possible to exclude the effect of different structural positions on the collected data. On the contrary, it is not possible to exclude the occurrence of rapid changes of fault core thickness in the direction perpendicular to the exposures due to other factors (Miller, 1996).

A further source of uncertainty for the models discussed in Figs. 9c and d and 10 is the unknown displacement of faults. Although these models are based on the reasonable and elsewhere documented assumption of a direct relationship between fault displacement and fault rock comminution, further field data and experiments are required to support or refute the discussed models at least for the section about the dependence upon the fault displacement. Moreover, consider that models of Figs. 9c and d and 10 are mostly based on the relationship between the normalised gouge zone thickness and the corresponding gouge *D*-values (Fig. 8a). In this paper, this relationship holds true for: (1) strike-slip fault cores occurring in platform limestone, (2) gouge zone thickness between ~0.02 and ~0.40 m, and (3) fault core thickness between ~0.04 and ~0.90 m. Whether the relationship of Fig. 8a provides valuable contributions to the explanation of the growth of fault cores in other settings, lithologies and fault core size ranges remain to be validated by further evidence.

An important uncertainty in the definition of grain size distributions of carbonate fault rocks may be the effect of possible pressure solution processes (Hadizadeh, 1994). Chemical analyses to determine this factor were not performed so, therefore, remains undefined. However, in the analysed fault cores, the lack of transgranular stylolites (Fig. 4) suggests that the effect of pressure solution was possibly minimised. In addition, the typical sealing capacity of fine-grained gouges (Antonellini and Aydin, 1994) may have inhibited carbonate dissolution in the fault cores (i.e. by impeding mass transfer through solute transport, e.g. Gratier, 1983) at least in the advanced stages of cataclasis when gouge material developed.

6. Conclusions

(1) Ten exposure-scale strike-slip fault cores developed in Mesozoic platform limestone within a regional fault zone show the same asymmetrical structural architecture consisting of a boundary fault surface, a gouge zone and a breccia zone, but different thickness and grain size distribution of the fault core components (i.e. breccia and gouge zones).
(2) The grain size distributions of fault core rocks are power-law over the 0.4–0.125 mm size range and have fractal dimensions (*D*) between ~2 and ~3.
(3) The fault cores evolve by grain comminution mostly consisting of early bulk crushing and late abrasion of grains, ultimately leading to the consumption of breccia material in favour of fault gouge.

Acknowledgements

F. Salvini and F. Storti are thanked for insightful discussions about fault rocks during previous works. D. Peacock is thanked for several comments and for a critical reading of an early version of the manuscript. C. Wibberley and an anonymous reviewer provided insightful comments.

References

Abe, S., Mair, K., 2005. Grain fracture in 3D numerical simulations of granular shear. Geophysical Research Letters 32, L05305. doi:10.1029/2004GL022123.

Allègre, C.J., Le Mouel, J.L., Provost, A., 1982. Scaling rules in rock fracture and possible implications for earthquake prediction. Nature 297, 47–49.

Amitrano, D., Schmittbuhl, J., 2002. Fracture roughness and gouge distribution of a granite shear band. Journal of Geophysical Research 107 (B12), 2375. doi:10.1029/2002JB001761.

Antonellini, M., Aydin, A., 1994. Effect of faulting on fluid flow in porous sandstones: petrophysical properties. American Association of Petroleum Geologists Bulletin 78, 355–377.

Aydin, A., 1978. Small faults formed as deformation bands in sandstone. Pure and Applied Geophysics 116, 913–930.

Beeler, N.M., Tullis, T.E., Blanpied, M.L., Weeks, J.D., 1996. Frictional behavior of large displacement experimental faults. Journal of Geophysical Research 101, 8697–8715.

Ben-Zion, Y., Sammis, C.G., 2003. Characterization of fault zones. Pure and Applied Geophysics 160, 677–715.

Billi, A., Storti, F., 2004. Fractal distribution of particle size in carbonate cataclastic rocks from the core of a regional strike–slip fault zone. Tectonophysics 384, 115–128.

Billi, A., Salvini, F., Storti, F., 2003a. The damage zone-fault core transition in carbonate rocks: implications for fault growth, structure and permeability. Journal of Structural Geology 25, 1779–1794.

Billi, A., Storti, F., Salvini, F., 2003b. Particle size distributions of fault rocks and fault transpression: are they related? Terra Nova 15, 61–66.

Blenkinsop, T.G., 1991. Cataclasis and processes of grain size reduction. Pure and Applied Geophysics 136, 59–86.

Brankman, C.M., Aydin, A., 2004. Uplift and contractional deformation along a segmented strike-slip fault system: the Gargano Promontory, southern Italy. Journal of Structural Geology 26, 807–824.

Byerlee, J.D., Summers, R., 1976. A note on the effect of fault gouge thickness on fault stability. International Journal of Rock Mechanics and Mining Sciences and Geomechanics Abstracts 13, 35–36.

Caine, J.S., Evans, J.P., Forster, C.B., 1996. Fault zone architecture and permeability structure. Geology 24, 1025–1028.

Chester, F.M., Logan, J.M., 1986. Implications for mechanical properties of brittle faults from observations of the Punchbowl fault zone, California. Pure and Applied Geophysics 124, 77–106.

Chester, F.M., Evans, J.P., Biegel, R.L., 1993. Internal structure and weakening mechanisms of the San Andreas Fault. Journal of Geophysical Research 98, 771–786.

Cladouhos, T.T., 1999. Shape preferred orientations of survivor grains in fault gouge. Journal of Structural Geology 21, 419–436.

Di Toro, G., Goldsby, D.L., Tullis, T.E., 2004. Friction falls towards zero in quartz rock as slip velocity approaches seismic rates. Nature 427, 436–439.

Engelder, T., 1974. Cataclasis and the generation of fault gouge. Geological Society of America Bulletin 85, 1515–1522.

Evans, J.P., Forster, C.B., Goddard, J.V., 1997. Permeability of fault-related rocks, and implications for hydraulic structure of fault zones. Journal of Structural Geology 19, 1393–1404.

Frye, K., Marone, C., 2002. The effect of particle dimensionality on granular friction in laboratory shear zones. Geophysical Research Letters 29, 1916. doi:10.1029/2002GL015709.

Graham, B., Antonellini, M., Aydin, A., 2003. Formation and growth of normal faults in carbonates within a compressive environment. Geology 31, 11–14.

Gratier, J.P., 1983. Estimation of volume changes by comparative chemical analyses in heterogeneously deformed rocks (folds with mass transfer). Journal of Structural Geology 5, 329–339.

Hadizadeh, J., 1994. Interaction of cataclasis and pressure solution in a low-temperature carbonate shear zone. Pure and Applied Geophysics 143, 255–280.

Hattori, I., Yamamoto, H., 1999. Rock fragmentation and grain size in crushed zones by faulting. Journal of Geology 107, 209–222.

Hooke, R.LeB., Iverson, N.R., 1995. Grain size distribution in deforming subglacial tills: role of grain fracture. Geology 23, 57–60.

House, W.M., Gray, D.R., 1982a. Cataclasites along the Saltville thrust, U.S.A., and their implications for thrust-sheet emplacement. Journal of Structural Geology 4, 257–269.

House, W.M., Gray, D.R., 1982b. Displacement transfer at thrust terminations in Southern Appalachians–Saltville Thrust as an example. American Association of Petroleum Geologists Bulletin 66, 830–842.

Hull, J., 1988. Thickness–displacement relationships for deformation zones. Journal of Structural Geology 10, 431–435.

Kim, Y.-S., Peacock, D.C.P., Sanderson, D.J., 2004. Fault damage zones. Journal of Structural Geology 26, 503–517.

Krumbein, W.C., Pettijohn, F.C., 1938. Manual of Sedimentary Petrography. Appleton-Century-Crotts Inc, New York.

Mancini, E.A., Blasingame, T.A., Archer, R., Panetta, B.J., Llinás, J.C., Haynes, C.D., Benson, D.J., 2004. Improving recovery from mature oil fields producing from carbonate reservoirs: Upper Jurassic Smackover Formation, Womack Hill field (eastern Gulf Coast, U.S.A.). American Association of Petroleum Geologists Bulletin 88, 1629–1651.

Mandl, G., de Jong, L.N.J., Maltha, A., 1977. Shear zones in granular material—an experimental study of their structure and mechanical genesis. Rock Mechanics 9, 95–144.

Marone, C., Scholz, C.H., 1989. Grain-size distribution and microstructures within simulated fault gouge. Journal of Structural Geology 11, 799–814.

Miller, M.G., 1996. Ductility in fault gouge from a normal fault system, Death Valley, California: a mechanism for fault-zone strengthening and relevance to paleoseismicity. Geology 24, 603–606.

Miller, S.A., Collettini, C., Chiaraluce, L., Cocco, M., Barchi, M., Kaus, B.J.P., 2004. Aftershocks driven by a high-pressure CO_2 source at depth. Nature 427, 724–727.

Monzawa, N., Otsuki, K., 2003. Comminution and fluidization of granular fault materials: implications for fault slip behavior. Tectonophysics 367, 127–143.

Morgan, K.J., Cladouhos, T.T., Scharer, K.M., Cowan, D.S., Vrojlik, P., 1996. Fractal grain size distributions in Death Valley fault zones: controls on mechanics and kinematics of fault rocks. Abstracts of Proceedings, EOS Transactions, AGU Fall Meeting, San Francisco.

Ramsay, J.G., 1980. Shear zone geometry: a review. Journal of Structural Geology 2, 83–99.

Salvini, F., Billi, A., Wise, D.U., 1999. Strike-slip fault-propagation cleavage in carbonate rocks: the Mattinata Fault zone. Journal of Structural Geology 21, 1731–1749.

Sammis, C.G., Osborne, R.H., Anderson, J.L., Banerdt, M., White, P., 1986. Self-similar cataclasis in the formation of fault gouge. Pure and Applied Geophysics 124, 53–78.

Sammis, C.G., King, G., Biegel, R., 1987. The kinematics of gouge deformation. Pure and Applied Geophysics 125, 777–812.

Scholz, C.H., 1987. Wear and gouge formation in brittle faulting. Geology 15, 493–495.

Scott, D.R., Marone, C., Sammis, C.G., 1994. The apparent friction of granular fault gouge in sheared layers. Journal of Geophysical Research 99, 7231–7246.

Sibson, R.H., 1986. Brecciation processes in fault zones: inferences from earthquake rupturing. Pure and Applied Geophysics 124, 159–176.

Sibson, R.H., 2003. Thickness of the seismic fault zones. Bulletin of the Seismological Society of America 93, 1169–1178.

Storti, F., Billi, A., Salvini, F., 2003. Grain size distributions in natural carbonate fault rocks: insights for non-self-similar cataclasis. Earth and Planetary Science Letters 206, 173–186.

Tarasewicz, J.P.T., Woodcock, N.H., Dickson, J.A.D., 2005. Carbonate dilation breccias: examples from the damage zone to the Dent Fault, northwest England. Geological Society of America Bulletin 117, 736–745.

Turcotte, D.L., 1986. Fractals and fragmentation. Journal of Geophysical Research 91, 1921–1926.

Wibberley, C.A.J., Shimamoto, T., 2003. Internal structure and permeability of major strike-slip fault zones: the Median Tectonic Line in Mie Prefecture, Southwest Japan. Journal of Structural Geology 25, 59–78.

Wibberley, C.A.J., Petit, J.-P., Rives, T., 2000. Micromechanics of shear rupture and the control of normal stress. Journal of Structural Geology 22, 411–427.

Wilson, B., Dewers, T., Reches, Z., Brune, J., 2005. Particle size and energetics of gouge from earthquake rupture zones. Nature 434, 749–752.